Metabolomic Serum Profiling After ACL Injury in Rats: A Pilot Study Implicating Inflammation and Immune Dysregulation in Post-Traumatic Osteoarthritis

Tristan Maerz,[1,2] Eric Sherman,[3] Michael Newton (iD),[2] Ali Yilmaz,[3] Praveen Kumar,[3] Stewart F. Graham,[3] Kevin C. Baker[2]

[1]Department of Orthopaedic Surgery, University of Michigan, Ann Arbor, Michigan, [2]Beaumont Research Institute, Orthopaedic Research Laboratories, Royal Oak, Michigan, [3]Beaumont Research Institute, Metabolomics Division, OB/GYN, Royal Oak, Michigan

ABSTRACT: ACL rupture is a major risk factor for post-traumatic osteoarthritis (PTOA) development. Little information exists on acute systemic metabolic indicators of disease development. Thirty-six female Lewis rats were randomized to Control or noninvasive anterior cruciate ligament rupture (ACLR) and to three post-injury time points: 72 h, 4 weeks, 10 weeks ($n = 6$). Serum was collected and analyzed by ^{1}H nuclear magnetic resonance (NMR) spectroscopy and combined direct injection and liquid chromatography (LC)-mass spectrometry (MS)/MS (DI-MS). Univariate and multivariate statistics were used to analyze metabolomic data, and predictive biomarker models were analyzed by receiver operating characteristic (ROC) analysis. Topological pathway analysis was used to identify perturbed pathways. Two hundred twenty-two metabolites were identified by ^{1}H NMR and DI-MS. Differences in the serum metabolome between ACLR and Control were dominated by medium- and long-chain acylcarnitine species. Further, decreases in several tryptophan metabolites were either found to be significantly different in univariate analysis or to play important contributory roles to multivariate model separation. In addition to acylcarnitines and tryptophan metabolites, glycine, carnosine, and D-mannose were found to differentiate ACLR from Control. Glycine, 9-hexadecenoylcarnitine, trans-2-Dodecenoylcarnitine, linoelaidyl carnitine, hydroxypropionylcarnitine, and D-Mannose were identified as biomarkers with high area under ROC curve values and high predictive accuracies. Our analysis provides new information regarding the potential contribution of inflammatory processes and immune dysregulation to the onset and progression of PTOA following ACL injury. As these processes have most commonly been associated with inflammatory arthropathies, larger-scale studies elucidating their involvement in PTOA development and progression are necessary. © 2018 Orthopaedic Research Society. Published by Wiley Periodicals, Inc. J Orthop Res 36:1969–1979, 2018.

Keywords: post-traumatic osteoarthritis; metabolomics; anterior cruciate ligament rupture; inflammation; immunity

Anterior cruciate ligament (ACL) rupture is a major risk factor for post-traumatic osteoarthritis (PTOA) development, and studies have demonstrated long-term incidences of PTOA following ACL rupture as high as 50–90%.[1–4] The ACL is a major stabilizer of the knee, and its rupture is associated with high-energy joint trauma. This initial trauma, subsequent joint laxity, persistent inflammation, and non-native joint kinematics after surgical reconstruction are among the most commonly proposed reasons for PTOA onset and progression.[1,2,5,6]

Relatively little is known about specific biological pathways responsible for the initiation and progression of ACL rupture-induced PTOA. Mechanobiological responses of the synovium, ACL, articular cartilage, and other tissues trigger the release of pro-inflammatory cytokines, proteases, and extracellular matrix (ECM) products,[5–11] initiating what is generally accepted as an irreversible, degenerative cascade.[1,12] Protein- and gene-level changes in the synovium following ACL rupture induce chronic synovitis,[13] a tissue condition characteristic of PTOA, and the synovium is known to be a major modulator of joint inflammation and catabolism.[13] Compositional and morphological adaptation occurs in subchondral and trabecular bone following ACL rupture,[14,15] and articular cartilage degeneration is thought to begin at the time of trauma, with processes responsible for chondrocyte apoptosis and altered protein expression initiated acutely after injury.[16] Although articular cartilage thinning and necrosis are generally attributed to the OA process, recent studies have demonstrated that both pathologic thinning and hypertrophic thickening occur following ACL rupture,[17–19] indicating dynamic, time-dependent processes during PTOA initiation and progression.

Given the plethora of biological processes potentially involved in PTOA, a need exists for more sensitive characterization of disease mechanisms that may be targeted for therapeutic intervention or improved, earlier diagnosis. An increasing number of publications have sought to identify biomarkers of PTOA, with numerous potential targets identified in urine, synovial fluid, and serum.[20] Metabolomics is a promising new technology enabling comprehensive and concurrent system-wide profiling of multiple metabolite concentrations in response to external stimuli including lifestyle, diet, disease, and genetic influences.[21] The major analytical methods used for high throughput metabolomics consist of ^{1}H nuclear magnetic resonance (^{1}H NMR) and mass spectrometry (usually with a chromatographic component), collectively providing complementary structural and conformational information on numerous compounds classes in a single analyses.[21] Data acquired via these platforms are increasingly popular, as evidenced by the

rise in the number of studies utilizing high resolution metabolomics platforms to identify metabolites and metabolic pathways associated with PTOA and OA progression.[22–25]

Most preclinical animal studies employ surgically induced models of PTOA (e.g., surgical ACL transection, medial meniscal destabilization), but these models may not accurately recapitulate the disease process in humans. With regards to metabolomics, these models could introduce confounding metabolites associated with surgical trauma, precluding accurate characterization of the pathology. In contrast, noninvasive injury models more accurately reproduce high-energy joint loading and induce a closed, clinically relevant injury, representing a more useful tool to study metabolic pathways. Our group recently developed and characterized a tibial compression model to induce closed, isolated ACL rupture in the rat.[26] This injury leads to drastic morphological tissue changes representative of PTOA.[14,17] The purpose of this pilot study was to employ this model in combination with high-resolution ^{1}H NMR and MS to study serum-levelmetabolic changes in the acute and intermediate post-injury timeframe of PTOA onset and progression.

MATERIALS AND METHODS
Treatment Groups, Noninvasive ACL Injury, and Specimen Collection
Under an IACUC-approved protocol, 36 female Lewis rats aged 14 weeks, ~200 g (Charles River Laboratories, Wilmington, MA) were acclimated to a 12-h light/dark facility for 1 week. Using a computer algorithm, rats were randomized to a control group (anesthesia and analgesia only, no injury loading) or noninvasive ACL rupture (ACLR) group. Rats were then further randomized to three time points: 72 h, 4 weeks, and 10 weeks ($n = 6$ rats per group per time point). Throughout the study, rats were allowed ad libitum cage activity and provided unlimited access to food and water. ACLR rats were subjected to a tibial compression-based noninvasive ACL rupture protocol, as previously described.[14,17,26] Briefly, rats were immobilized in prone position on a custom fixture on a materials testing system (Insight 5, MTS Systems, Eden Prairie, MN). The right knee was flexed to 100° and constrained to restrict medial and lateral translation, and the right paw was mounted in 30° of dorsiflexion. After a preloading and preconditioning, a displacement of 3 mm was rapidly applied to the paw at a rate of 8 mm/s, causing anterior tibial subluxation and subsequent failure of the ACL.[26] Anesthesia was induced with intraperitoneal ketamine/xylazine and maintained with 1–2% inhaled isoflurane. Subcutaneous carprofen was administered for preemptive analgesia, and subcutaneous buprenorphine for post-injury analgesia. Characterization studies of bony remodeling,[14] articular cartilage degeneration with documented worsening histologic grade (OARSI score of ~12 at 4 and 10 weeks),[17] and acute stem cell migration[27] have been published on the same rats utilized in this study and can be referenced for further information on downstream joint changes and cellular phenomena.

At respective 72-h, 4-, and 10-week time points, whole blood was collected via cardiac puncture and rats were euthanized by CO_2 asphyxia. Serum was obtained via centrifugation at 1,200g at 4°C for 10 mins, aliquoted, and stored at −80°C until processing.

^{1}H NMR Sample Preparation and Data Acquisition
Serum specimens were prepared as described by Mercier et al.[28] Briefly, 3 KDa cut-off centrifugal filter units (Amicon Microcon YM-3; Sigma–Aldrich, St. Louis, MO) were rinsed seven times by centrifugation (12,000g for 30 min) using 0.5 ml of H_2O to remove residual glycerol. Subsequently, 250 µl of rat serum was transferred to the filter units and centrifuged at 13,000g for 30 min at 4°C. 200 µl of filtered serum was combined with 25 µl of D_2O and 21 µl of standard buffer solution consisting of 11.7 mM DSS [disodium-2,2-dimethyl-2-silapentane-5-sulphonate], 1.75 M K_2HPO_4, and 5.84 mM 2-chloro pyrimidine-5-carboxylic acid (phasing standard) in H_2O. Using an Eppendorf liquid handler, 200 µl were transferred to 3 mm NMR tubes for analysis by NMR.

All ^{1}H-NMR experiments were recorded at 300.0 K (±0.05) using a Bruker Avance III HD 600 MHz spectrometer coupled with a 5 mm TCI cryoprobe (Bruker-Biospin, Billerica, MA). Using a randomized running order, 1D ^{1}H NMR spectra were acquired using a pulse sequence developed by Ravanbakhsh et al.[29] Two hundred and fifty-six transients were acquired. DSS was used as the internal standard for chemical shift referencing and quantification. Collected spectra were analyzed using a custom library of 59 metabolites using Bayesil.[29]

Combined Direct Injection and LC-MS/MS (DI-MS) Compound Identification and Quantification
A comprehensive description of this analysis has been previously described by our group.[30] Briefly, targeted analysis was carried out using AbsoluteIDQ p180 kit (Biocrates Life Sciences AG, Innsbruck, Austria) on a TQ-S mass spectrometer coupled to an Acquity I Class ultra-pressure liquid chromatography (UPLC) system (Waters Technologies Corporation, Milford, MA). Serum samples were analyzed using the protocol described in AboluteIDQ manual.

Univariate and Multivariate Statistical Analyses
Univariate statistical analyses of all concentration data from ^{1}H-NMR and DI-MS were performed using SPSS (v22, IBM, Armonk, NY). Zero values were treated as missing values, and features with more than 50% missing values were excluded entirely. To assess differences in metabolite concentrations as a function of experimental group and time point, two-way analysis of variance (ANOVA) was used. Post hoc analysis of multiple comparisons was performed with the Sidak P-value correction. ANOVA assumptions were assessed using the Shapiro–Wilk test for normality and Levene's test for homogeneity of variances. Multivariate analyses of concentration data from ^{1}H-NMR and DI-MS were performed using Metaboanalyst 3.0, a free online analysis utility for metabolomics.[31,32] Data were normalized to the sum and scaled by unit variance. To assess major variation in the dataset and to identify outliers, unsupervised principal component analysis (PCA) was performed. Outliers were defined as samples outside the 95% confidence limit (Hotelling's T-squared distribution). Subsequently, supervised partial least squares discriminant analysis (PLS-DA) was utilized. Variable importance in projection (VIP) plots listing the top 15 metabolites were generated for each PLS-DA model. VIP scores estimate the relative importance of each metabolite in the projection of a PLS model, provid-

ing a quantitative parameter of a metabolite's importance in distinguishing between two groups. Analyses were performed between the two experimental groups at each time point. PLS-DA models were then validated using permutation testing (2000 iterations).

Biomarker and Pathway Topology Analysis

Data were analyzed using the Biomarker function in Metaboanalyst to determine which metabolite pairs would be best for developing predictive models for use as disease biomarkers. Predictive classification models were built using various combination pairs of the top five metabolites, identified using least absolute shrinkage and selection operator (LASSO) regression analysis.[33] Predictive models were developed using a PLS-DA algorithm as the classification method and feature ranking method. The performance of predictive models was assessed using Monte-Carlo cross validation (MCCV) with balanced subsampling, and the area under the receiver operating characteristic curve (AUROC) and predictive accuracy were calculated for each metabolite combination as measures of predictive ability.

Topological pathway analysis was performed in MetaboAnalyst to identify the most perturbed biological pathways, as previously described.[34,35] Briefly, the *Rattus Norvegicus* library was chosen, and the test for pathway enrichment analysis and relative-betweenness centrality options for the pathway topology analyses were selected. Significance was set at $p < 0.1$.

RESULTS

We accurately identified and quantified 58 metabolites using ^{1}H NMR and 186 using DI-MS (Fig. 1). Some overlap was observed between the two platforms (22 metabolites) and as such, we took the average values for each individual metabolite measured using both analytical methods, yielding 222 unique metabolites (Supplemental Data, Table S1).

Univariate Comparisons

Based on two-way ANOVA of raw data, 17 metabolites were found to be significantly different between ACLR and Control ($p < 0.05$ after Sidak correction) at 72 h (Table 1). At 4 weeks, 8 metabolites had significantly different concentrations, and at 10 weeks, 3 metabolites were found to have significantly different concentrations (Table 1).

Multivariate Modeling

Unsupervised PCA modeling did not identify any significant outliers. The total percentage of explained variation by the first three principal components was 65.5% at 72 h, 70.9% at 4 weeks, and 71.5% at 10 weeks. No notable separation was observed in any of the PCA models. (Supplemental Data, Fig. S1).

Table 1. Metabolites With Significantly Different Concentrations Between Control and ACLR Based on Univariate Two-Way Anova at 72 Hours, 4 Weeks, and 10 Weeks

| Time Point	Metabolite	Control (µM ± SD)	ACLR (µM ± SD)	Fold-Change	p-Value
72 hours	L-Aspartic acid	102.73 ± 41.99	62.90 ± 21.58	0.612	0.002
	C5-DC/C6-OH	0.0238 ± 7.33E-3	0.013 ± 0.007	0.542	0.005
	Carnosine	2.561 ± 1.805	0.452 ± 0.304	0.177	0.007
	1-Phenylethylamine	6.517 ± 5.152	2.353 ± 3.687	0.361	0.009
	N-Acetylornithine	3.063 ± 0.697	2.100 ± 0.511	0.685	0.011
	Succinic acid	610.23 ± 396.11	300.70 ± 129.85	0.493	0.011
	C16-OH	0.00783 ± 4.08E-4	0.0130 ± 0.007	1.639	0.016
	Formic acid	87.50 ± 38.71	48.05 ± 18.87	0.549	0.021
	Fumaric acid	17.51 ± 7.413	9.750 ± 4.207	0.556	0.023
	C5-OH/C3-DC-M	0.0972 ± 0.0253	0.0730 ± 0.0160	0.751	0.023
	Serotonin	2.322 ± 1.324	1.023 ± 0.442	0.441	0.031
	L-Carnitine	48.20 ± 8.768	38.16 ± 9.988	0.792	0.034
	Spermidine	77.15 ± 117.10	189.20 ± 180.15	2.451	0.038
	3,5-Tetradecadiencarnitine	0.0107 ± 2.34E-3	0.0157 ± 6.41E-3	1.468	0.041
	Isopropyl alcohol	49.56 ± 23.51	78.45 ± 26.07	1.582	0.043
	H1	12811 ± 2613	10132 ± 2479.0	0.791	0.048
	3-Nitrotyrosine	0.831 ± 0.229	0.680 ± 0.209	0.818	0.048
4 weeks	Serotonin	3.460 ± 1.470	1.840 ± 0.470	0.531	0.006
	Linoelaidyl carnitine	0.0250 ± 0.004	0.0140 ± 0.007	0.586	0.008
	trans-2-Dodecenoylcarnitine	0.216 ± 0.035	0.3200 ± 0.044	1.479	0.008
	L-Palmitoylcarnitine	0.170 ± 0.046	0.116 ± 0.020	0.683	0.012
	Stearoylcarnitine	0.100 ± 0.050	0.063 ± 0.009	0.636	0.013
	Oleoylcarnitine	0.100 ± 0.0220	0.0707 ± 0.0143	0.705	0.027
	9-Decenoylcarnitine	0.218 ± 0.031	0.313 ± 0.041	1.433	0.030
	PC16:0/16:0	20.13 ± 16.48	10.68 ± 2.017	0.531	0.034
10 weeks	Butyrylcarnitine	2.320 ± 1.30	6.960 ± 0.32	2.994	0.016
	Hexanoylcarnitine	0.129 ± 0.055	0.470 ± 0.32	3.650	0.020
	Hydroxypropionylcarnitine	9.00E-3 ± 8.36E-3	1.33E-3 ± 1.75E-3	0.176	0.024
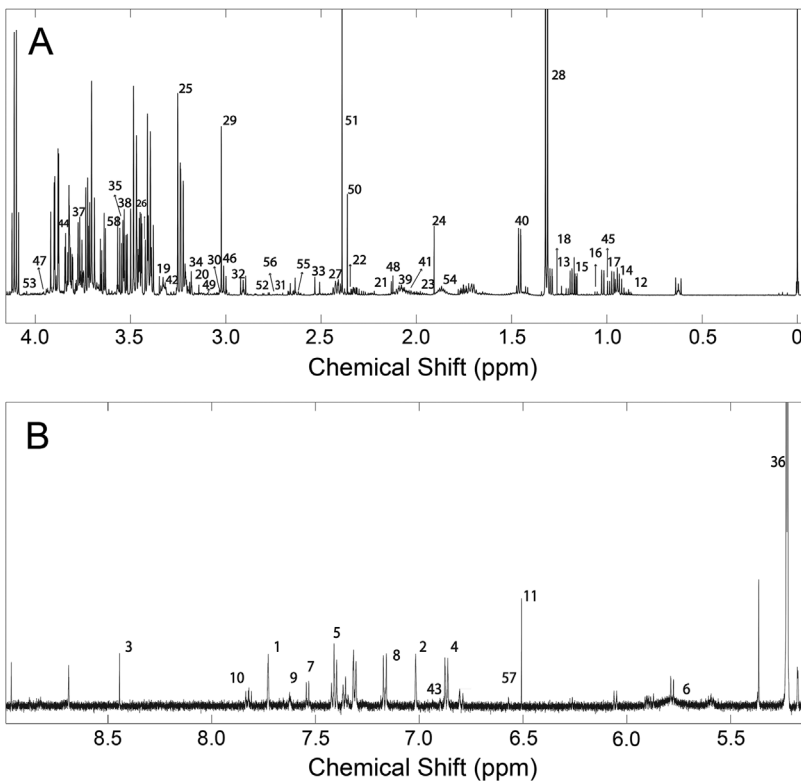
Figure 1. A representative 1D ^{1}H NMR spectrum of serum used in this study. (A) Aliphatic region; (B) Aromatic region. 1. Histidine, 2. 1-methylhistidine, 3. Formate, 4. Tyrosine, 5. Phenylalanine, 6. Urea, 7. Hippurate, 8. Tryptophan, 9. 3-Methylhistidine, 10. Xanthine, 11. Fumarate, 12. 2-Hydroxybutyrate, 13.3-Hydroxybutyrate, 14. Leucine, 15. Isopropanol, 16. Isobutyrate, 17. Valine, 18. Propylene glycol, 19. Methanol, 20. Dimethyl sulfone, 21. Acetone, 22. 3-Hydroxyisovalerate, 23. Isovalerate, 24. Acetate, 25. Betaine, 26. Acetoacetate, 27. Carnitine, 28 Lactate, 29. Creatine, 30. Creatinine, 31. Dimethylamine, 32. Dimethylglycine, 33. Citratel, 34. Choline, 35. Ethanol, 36. Glucose, 37. Glycerol, 38. Glycine, 39. Glutamate, 40. Alanine, 41. Proline, 42. Threonine, 43. Asparagine, 44. Mannose, 45. Isoleucine, 46. Lysine, 47. Serine, 48. Methionine, 49. Malonate, 50. Pyruvate, 51. Succinate, 52. Aspartate, 53. Myo-inositol, 54. Ornithine, 55. Pyroglutamate, 56. Sarcosine, 57. Arginine 58. Glutamine.

Subsequently, supervised PLS-DA modeling was applied, which yielded marked group separation between Control and ACLR at 72 h (Fig. 2A) and 4 weeks (Fig. 2C), and modest separation at 10 weeks (Fig. 2E). Despite this observed separation, given the relatively small sample size ($n = 6$), these models were not found to be significant following cross validation using 2000 iterations of permutation testing (72 h: $p = 0.760$; 4 weeks: $p = 0.999$; 10 weeks: $p = 0.928$). VIP plots of respective models at each time point indicate the top 15 most contributory metabolites responsible for group separation (Fig. 2B, D, F). At 72 h, increases in the concentrations of glycine and 9-hexadecenoylcarnitine, and decreases in carnosine were the three most-contributory metabolite features separating Control and ACLR (Fig. 2B). Based on univariate analyses, there were no significant differences in the concentrations of glycine (Control: 195.7 μM ± 32.5, ACLR: 214.5 μM ± 20.2, $p = 0.201$) or 9-hexadecenoylcarnitine (Control: 25.8 nM ± 6.14, ACLR: 30.5 nM ± 2.42, $p = 0.182$), but a significant difference in carnosine concentration was observed (Control: 2.56 μM ± 1.80, ACLR: 0.452 μM ± 0.304, $p = 0.007$). In addition to these three metabolites, fumaric acid (Control: 17.51 μM ± 7.41, ACLR: 9.750 μM ± 4.20, $p = 0.023$), isopropyl alcohol (Control: 49.56 μM ± 23.51, ACLR: 78.45 μM ± 26.07, $p = 0.043$), and 3,5-Tetradecadiencarnitine (Control: 0.0107 μM ± 0.0023, ACLR: 0.0157 μM ± 0.0064, $p = 0.041$) had significantly different absolute concentrations based on univariate analyses and were in the top-15 highest VIP scores (Fig. 2B).

At 4 weeks post-injury, the VIP plot demonstrates that increases in the concentrations of trans-2-dodecenoylcarnitine, acetic acid, and 9-decenoylcarnitine were the three most contributory features to group separation (Fig. 2D). There were significant univariate differences in the concentrations of trans-2-dodecenoylcarnitine (Control: 0.216 μM ± 0.035, ACLR: 0.320 μM ± 0.044, $p = 0.008$) and 9-decenoylcarnitine (Control: 0.218 μM ± 0.031, ACLR: 0.313 μM ± 0.041, $p = 0.012$) but not in acetic acid concentration (Control: 73.43 μM ± 12.1, ACLR: 89.61 μM ± 17.4, $p = 0.306$). Furthermore, Linoelaidyl carnitine (Control: 0.025 μM ± 0.004, ACLR: 0.014 μM ± 0.007, $p = 0.008$), serotonin (Control: 3.460 μM ± 1.47, ACLR: 1.840 μM ± 0.470, $p = 0.006$), and L-Palmitoylcarnitine (Control: 0.170 μM ± 0.046, ACLR: 0.116 μM ± 0.020, $p = 0.012$) had significant differences in absolute concentrations and were in the top-15 highest VIP scores (Fig. 2D).

At 10 weeks, VIP plots indicate that a decrease in D-Mannose concentration and increases in hexanoylcarnitine and butyrylcarnitine concentrations were the three most contributory features separating Control and ACLR (Fig. 2F). There was a trending univariate difference in D-Mannose concentration between Control and ACLR (Control: 75.93 μM ± 26.4, ACLR: 31.98 μM ± 25.1, $p = 0.076$) and significant differences in the concentrations of hexanoylcarnitine (Control: 0.129 μM ± 0.055, ACLR: 0.470 μM ± 0.322, $p = 0.020$) and butyrylcarnitine (Control: 2.325 μM ± 1.30, ACLR: 6.965 μM ± 4.69, $p = 0.016$). In addition, Hydroxypropionylcarnitine (Control: 9.00 nM ± 8.36, ACLR: 1.33 nM ± 1.75, $p = 0.024$) had significantly different
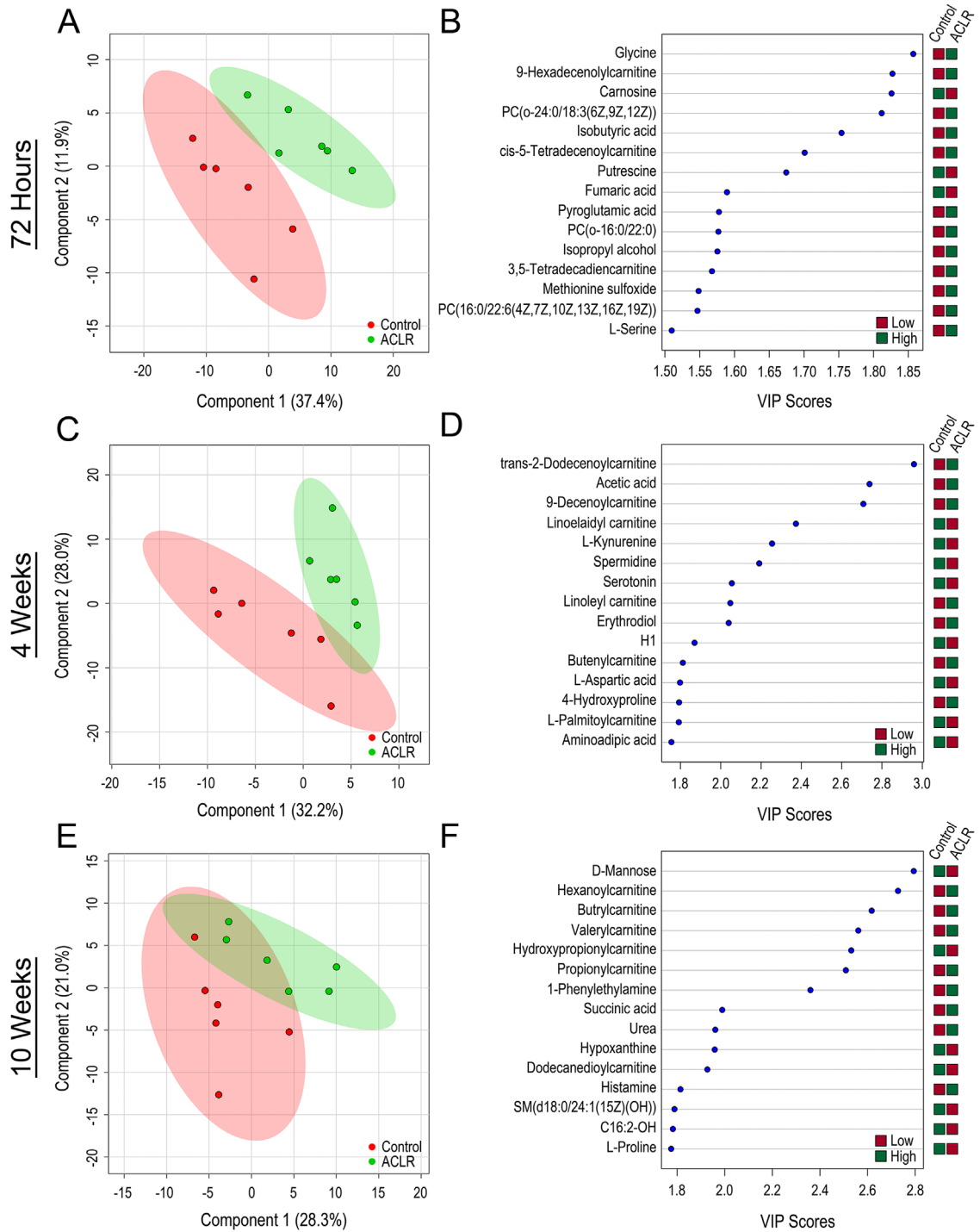
Figure 2. PLS-DA scores plots (A, C, E) and corresponding VIP plots (B, D, F) of Control and ACLR rats at 72 h, 4 weeks, and 10 weeks. Shaded regions on PLS-DA plots correspond to the 95% confidence interval region. VIP plots rank metabolites by VIP score, a quantitative parameter of a given metabolite's importance in observed group separation (i.e., projection of the PLS-DA model).

absolute concentration between Control and ACLR and were in the top-15 highest VIP scores (Fig. 2F).

Predictive Biomarker Models

Having established which metabolites had the greatest absolute concentration differences and contributed most notably to group separation of multivariate models (i.e., highest VIP scores), we used LASSO regression to identify five metabolites at each time point, and predictive models were built to determine the predictive ability of combination pairs of the five identified metabolites as potential biomarkers of PTOA onset and progression (Table 2 and Fig. 3). At 72 h, Glycine, 9-Hexadecenoylcarnitine, Fumaric acid, Methionine sulfoxide, and PC(o-24:0/18:3(6Z,9Z,12Z)) were selected for biomarker analysis. AUROC values

Table 2. Area Under the Receiver Operating Characteristic Curve (AUROC) With 95% CIs and Predictive Accuracy (PA) of Metabolite Pairs Used to Develop Predictive Biomarker Models

Time Point	Metabolite 1	Metabolite 2	AUROC (95%CI)	PA
72 hours	Glycine	9-Hexadecenoyl-carnitine	0.952 (0.75–1.00)	76.8%
		Fumaric acid	0.912 (0.75–1.00)	82.0%
		Methionine sulfoxide	0.908 (0.50–1.00)	70.2%
		PC(o-24:0/18:3(6Z,9Z,12Z))	0.925 (0.62–1.00)	77.8%
	9-Hexanedecenoyl-carnitine	Fumaric acid	0.895 (0.50–1.00)	78.8%
		Methionine sulfoxide	0.938 (0.50–1.00)	76.8%
		PC(o-24:0/18:3(6Z,9Z,12Z))	0.925 (0.50–1.00)	82.0%
	Fumaric acid	Methionine sulfoxide	0.860 (0.50–1.00)	71.0%
		PC(o-24:0/18:3(6Z,9Z,12Z))	0.848 (0.50–1.00)	70.2%
	Methionine sulfoxide	PC(o-24:0/18:3(6Z,9Z,12Z))	0.942 (0.75–1.00)	81.8%
4 weeks	trans-2-Dodecenoylcarnitine	9-Decenoylcarnitine	0.828 (0.50–1.00)	66.8%
		Acetic acid	0.910 (0.25–1.00)	82.5%
		Serotonin	0.998 (1.00–1.00)	93.0%
		Linoelaidyl carnitine	0.998 (1.00–1.00)	96.8%
	9-Decenoylcarnitine	Acetic acid	0.830 (0.25–1.00)	79.0%
		Serotonin	0.998 (1.00–1.00)	94.5%
		Linoelaidyl carnitine	0.962 (0.50–1.00)	91.0%
	Acetic acid	Serotonin	0.938 (0.62–1.00)	83.2%
		Linoelaidyl carnitine	0.912 (0.50–1.00)	82.0%
	Serotonin	Linoelaidyl carnitine	0.770 (0.25–1.00)	66.2%
10 weeks	Hydroxypropionylcarnitine	D-Mannose	0.965 (0.50–1.00)	87.8%
		Formic acid	0.875 (0.50–1.00)	78.0%
		Hexanoylcarnitine	0.900 (0.50–1.00)	77.5%
		Propionylcarnitine	0.910 (0.50–1.00)	78.2%
	D-Mannose	Formic acid	0.712 (0.25–1.00)	69.2%
		Hexanoylcarnitine	0.840 (0.50–1.00)	75.7%
		Propionylcarnitine	0.840 (0.50–1.00)	72.0%
	Formic acid	Hexanoylcarnitine	0.740 (0.25–1.00)	67.0%
		Propionylcarnitine	0.745 (0.12–1.00)	65.8%
	Hexanoylcarnitine	Propionylcarnitine	0.780 (0.25–1.00)	70.5%

of combination pairs ranged from 0.848 to 0.952, and predictive accuracies of these models following 100-fold cross validation ranged from 71.0% to 82.0% (Table 2). The combination of Glycine and 9-Hexadecenoylcarnitine generated the model with the highest AUROC of 0.952 (95%CI 0.75–1.00) (Fig. 3A), and this model had a predictive accuracy of 76.8%. At 4 weeks, trans-2-Dodecenoylcarnitine, 9-Decenoylcarnitine, Acetic acid, Serotonin, and Linoelaidyl carnitine were selected for biomarker analysis. AUROC values of metabolite pairs at 4 weeks ranged from 0.770 to 0.998, and following 100-fold cross validation, predic-
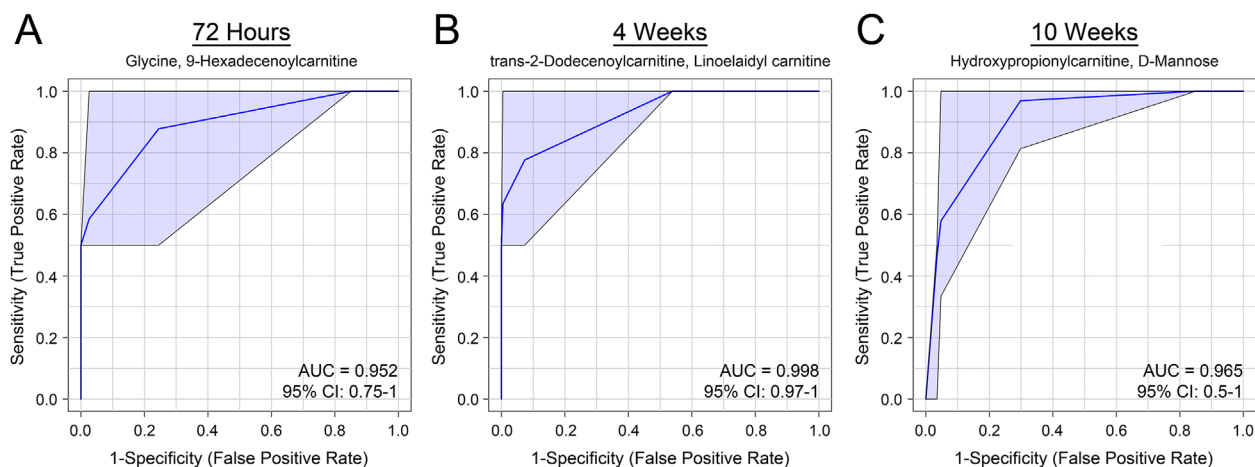
Figure 3. ROC curves of metabolite pairs used for predictive modeling at 72 h (A), 4 weeks (B), and 10 weeks (C).

tive accuracies ranged from 66.8% to 96.8% (Table 2). The combination of trans-2-Dodecenoylcarnitine and Linoelaidyl carnitine produced the model with the highest AUROC of 0.998 (95%CI 1.00–1.00) (Fig. 3B), and this model had a predictive accuracy of 96.8%. At 10 weeks, Hydroxypropionylcarnitine, D-Mannose, Formic acid, Hexanoylcarnitine, and Propionylcarnitine were selected as the top five metabolites for biomarker analysis. Combinations of these five metabolites generated AUROC values ranging from 0.712 to 0.975, with predictive accuracies following 100-fold cross validation found to range from 65.8% to 87.8% (Table 2). The combination of Hydroxypropionylcarnitine and D-Mannose produced the model with the highest AUROC of 0.975 (95%CI 0.50–1.00) (Fig. 3C), and this combination had a predictive accuracy of 87.8%.

Pathway Analysis

Topological pathway analysis revealed several perturbed biochemical pathways due to alterations in metabolite concentration after ACL injury (Table 3). At 72 h, 12 pathways were significantly perturbed ($p \leq 0.1$). The most significantly affected pathways at 72 h were cyanoamino acid metabolism ($p = 0.017$),

methane metabolism ($p = 0.030$), sphingolipid metabolism ($p = 0.031$), histidine metabolism ($p = 0.033$), and glutathione metabolism ($p = 0.033$). At 4 weeks, Tryptophan metabolism ($p = 0.063$) and β-Alanine metabolism ($p = 0.081$) were significantly perturbed, and at 10 weeks, fructose and mannose metabolism ($p = 0.020$) and amino sugar and nucleotide sugar metabolism ($p = 0.020$) were significantly perturbed.

DISCUSSION

Despite the increasing incidence of PTOA in both military and civilian populations,[36] the exact mechanisms connecting joint trauma to the onset and progression of joint degeneration are poorly understood. Evidence supporting the existence of underlying acute biologic phenomena at the time of ACL injury that precipitate rapid joint degeneration continues to emerge.[5,6] In the present study, we applied high-resolution ^{1}H-NMR spectroscopy and DI-MS to measure metabolite concentrations in the serum of rats subjected to a validated, non-surgical ACL rupture protocol.[26] We found that several carnitine and tryptophan metabolites distinguished ACLR from Control rats, and AUROC analysis of the top two LASSO regression-identified metabolites at each time point

Table 3. Results of Pathway Topology Analysis Indicating Perturbed Biochemical Pathways Been Control and ACLR Rats

Time Point	Pathway(s)	Total Compounds	Hits (Number of Hits)	p-Value
72 hours	Cyanoamino acid metabolism	6	Glycine, L-Serine (2)	0.017
	Methane metabolism	9	Glycine, Methanol, Formic acid, L-Serine (4)	0.030
	Sphingolipid metabolism	21	SM, L-Serine (2)	0.031
	Histidine metabolism	15	L-Glutamic acid, L-Histidine, Histamine, Carnosine, L-Aspartic acid, 1-Methylhistidine (6)	0.033
	Glutathione metabolism	26	L-Glutamic acid, Glycine, Pyroglutamic acid, Ornithine, Putrescine, Spermidine, Spermine (7)	0.033
	Porphyrin and chlorophyll metabolism	27	Glycine, L-Glutamic acid (2)	0.037
	Primary bile acid biosynthesis	46	Glycine, Taurine (2)	0.038
	Nitrogen metabolism	9	L-Glutamic acid, L-Glutamine, L-Histidine, Glycine (4)	0.053
	Propanoate metabolism	20	Succinic acid, 2-Hydroxybutyric acid (2)	0.063
	Purine metabolism	68	Xanthine, L-Glutamine, Urea (3)	0.075
	Arginine and proline metabolism	44	L-Glutamine, Ornithine, Citrulline, L-Aspartic acid, L-Arginine, L-Glutamic acid, N-Acetylornithine, L-Proline, Hydroxyproline, Creatine, Putrescine, Spermidine, Fumaric acid, Urea, Spermine (15)	0.075
	Glycine, serine, and threonine metabolism	32	L-Serine, Choline, Betaine, Dimethylglycine, Glycine, Sarcosine, L-Threonine, Creatine, Pyruvic acid (9)	0.087
4 weeks	Tryptophan metabolism	41	L-Tryptophan, Serotonin, L-Kynurenine (3)	0.063
	ß-Alanine metabolism	19	L-Aspartic acid, Spermidine, Spermine (3)	0.081
10 weeks	Fructose and mannose metabolism	19	D-Mannose (1)	0.020
	Amino sugar and nucleotide sugar metabolism	37	D-Mannose (1)	0.020

demonstrated predictive accuracies of 76.8%, 96.8%, and 87.8% at 72 h, 4 weeks and 10 weeks, respectively. These results demonstrate that the combined ^{1}H-NMR and DI-MS platforms are powerful techniques to identify biomarkers and potential biologic mechanisms underlying PTOA development.

VIP plots from PLS-DA modeling demonstrated that increased glycine and hexadecenoylcarnitine concentrations, along with decreased carnosine concentrations, were most contributory to distinguishing ACLR rats from Control rats at 72 h. At 4 weeks, increased concentrations of trans-2-dodecenoylcarnitine, acetic acid, and 9-decenoylcarnitine were the top three features, and at 10 weeks, decreased D-mannose and increased hexanoylcarnitine and butyrylcarnitine concentrations were most contributory to group separation. Mickiewicz et al. employed ^{1}H-NMR to characterize metabolites in synovial fluid 2 weeks after idealized ACL reconstruction procedure in sheep.[22] They found higher synovial fluid concentrations of isobutyrate and glucose in sheep that had undergone ACL reconstruction, while hydroxyproline, asparagine, serine, and uridine concentrations were lower. Similarly, we found that serum concentrations of L-serine and isobutyrate were increased in rats with an ACL rupture at the 72-h time point, though univariate analysis did not demonstrate significant concentration differences of these metabolites. Further, VIP analysis demonstrated that isobutyrate was among the key markers contributing to separation between the ACLR and Control group at the 72-h time point. In another study by Mickiewicz et al., a combined ^{1}H-NMR and GC-MS-based approach was used to measure metabolite concentrations in synovial fluid from patients with chronic knee osteoarthritis and healthy controls.[23] They identified the 11 metabolites most responsible for OPLS-DA separation between OA and Control synovial fluid, and our analysis identified one serum metabolite in common with the synovial fluid results of Mickiewicz et al.: The medium-chain acylcarnitine, hexanoylcarnitine.

At each time point, the serum concentration of several acylcarnitine species contributed significantly to PLS-DA separation. Acylcarnitines are fatty acid esters of L-carnitine which play important roles in energy production by promoting the entry of long chain fatty acids into the mitochondrion via the carnitine shuttle. Univariate analysis showed that free carnitine (L-carnitine) was significantly decreased in ACLR animals, while VIP analysis demonstrated that a total of 15 acylcarnitine species contributed substantially to model separation. Eight of these acylcarnitine species had significant univariate concentration differences between ACLR and Control, with five metabolites exhibiting increased and three metabolites displaying decreased concentrations. Low circulating levels of free carnitine and acylcarnitine species have been implicated in several immune/inflammatory conditions, including systemic lupus erythematous

(SLE)[37] and rheumatoid arthritis (RA).[38] Prior to definitive clinical onset of RA, Surowiec et al. observed a decrease in plasma acylcarnitines when compared to healthy controls.[39] Incomplete β-oxidation is implicated in the accumulation of esterified carnitine species, which may promote inflammation through the NF-κB pathway.[37] Zhang et al. defined OA phenotypes via metabolomic analyses and found that one specific phenotype was defined by differential expression of acylcarnitines,[40] though it was unclear if this was a post-traumatic OA phenotype. Adams et al. demonstrated that acylcarnitine species were significantly increased in the synovium of patients with end-stage knee osteoarthritis,[41] compared to patients with little evidence of OA that were undergoing surgery due soft tissue injury. Our present study indicates a strong influence from trans-2-docecenoylcarnitine at 4 weeks, with a 1.48-fold change relative to Control ($p = 0.008$), the highest VIP value in PLS-DA modeling, and a 96.8% predictive accuracy (AUROC = 0.998, 95%CI 0.97–1.00) when paired with linoelaidyl carnitine in predictive modeling. These results and findings from the aforementioned studies indicate that free- and esterified carnitine metabolites may play a role in OA/PTOA development.

Topological pathway analysis demonstrated several perturbed pathways due to ACLR (Table 3). One potentially important perturbed pathway in the context of arthritis was tryptophan metabolism. Several tryptophan metabolites were significantly different between ACLR and Controls at 72 h (decreased L-aspartic acid, 1-phenylethylamine, and serotonin concentrations). At 4 weeks, a decrease in L-kynurenine, serotonin, and L-aspartic acid were top VIP features, and at 10 weeks, an increase in 1-phenylethylamine was a top VIP feature. Kang et al. demonstrated that synovial fluid from patients with RA showed significantly lower concentrations of tryptophan metabolites,[42] including kynurenine, indoelactic acid, N'-Formylkynurenine and indoleacetaldehyde when compared to synovial fluid from OA patients. Kynurenine is an endogenous ligand for the aryl hydrocarbon receptor (AHR), and binding of AHR by kynurenine leads to production of T_{regs} and suppression of IL-17-producing Th cell populations.[43,44] Further, Chen et al. demonstrated that increasing kynurenine levels via indoleamine 2,3-dioxygenase (IDO)-targeted gene therapy promoted the resolution of collagen-induced arthritis,[45] primarily by apoptosis of T-cells and reduction in synovial IL-17. We previously demonstrated that our ACL injury model leads to acutely increased IL-17 expression in synovium.[27] Given the presently demonstrated reduction in tryptophan metabolites that could serve as AHR ligands in ACLR animals, we hypothesize that a pro-inflammatory environment is favored in the acute period after injury. Furthermore, the tryptophan metabolite serotonin has been closely linked with bone mineral density in the setting of osteoporosis[46] and with IL-17-associated osteoclasto-

genesis in autoimmune arthritis,[47] indicating that serotonin may play a role in the subchondral and epiphyseal bone remodeling we have observed following ACL rupture in this model.[14]

In addition to metabolites involved in carnitine and tryptophan metabolism, several other key metabolites contributed to the observed PLS-DA separation. At 72 h, glycine had the highest VIP score and was involved in the significant perturbation of several pathways (Table 3). Glycine has been recently implicated in muscle fibrosis in RA patients[48] and as an amino acid crucial for collagen synthesis, it may be linked to acute tissue remodeling in our model, but further experimentation is necessary to elucidate its precise role in PTOA. At 72 h, carnosine had the third-highest VIP rank and had significantly lower univariate concentrations in ACLR compared to Control ($p = 0.007$). Ponist et al. recently demonstrated that oral carnosine reduced edema in the paws of carrageenan-treated rats in adjuvant arthritis and further demonstrated reduced oxidative stress in primary culture of articular chondrocytes[49]—these findings may be an indication that reduced carnosine observed in our data is involved in post-injury inflammation. In addition, D-mannose was a strong contributor to model separation at 10 weeks, with a VIP value near 2.8 and a lower univariate concentration difference of trending significance ($p = 0.076$). Furthermore, D-mannose was a key metabolite in the significant perturbation of fructose and mannose metabolism ($p = 0.020$) and amino sugar and nucleotide sugar metabolism ($p = 0.020$). Mannose is a monosaccharide involved in protein N-glycosylation, which is integral to several physiologic functions including lectin-mediated cell-cell interactions. One hypothesis is that reduced serum mannose reflects consumption in N-glycosylation associated with stem and immune cell trafficking to the injured joint, which we have observed in this model.[27] Urita et al. described decreased concentrations of N-glycan species in both human and murine osteoarthritic articular cartilage and demonstrated a correlation between high mannose N-glycans and chondrocyte production of matrix-degrading enzymes MMP-13 and ADAMTS-5 in response to interleukin-1α stimulation.[50] Additional investigation into the roles of glycine, carnosine, and D-mannose in the onset and progression of ACL rupture-induced PTOA is warranted.

Our study is not without limitations. Our findings are limited by a small sample size ($n = 6$), and our PLS-DA models were not found to be significant. Nonetheless, as a preliminary investigation of the serum metabolome after ACL injury, we found several significant univariate differences, significantly perturbed pathways, and high AUROC and predictive accuracy values from predictive modeling. Another limitation is the lack of concomitant analysis of local joint tissue or synovial fluid—additional metabolic profiling of synovial fluid, synovial membrane, cartilage, and subchondral bone would provide a greater

understanding of local biochemical changes following ACL rupture. Although we performed a cross-sectional experiment to assess three distinct time points, we did not perform multivariate modeling as a function of time, which could characterize metabolites involved in disease progression. Future studies are planned to undertake more powered studies involving longitudinal multivariate analyses. Lastly, further characterization is warranted to determine whether the pattern of expression of the identified metabolites aids in distinguishing between PTOA, idiopathic osteoarthritis, and inflammatory arthropathies, which the present study did not address.

To our knowledge, this is the first high-resolution metabolomics characterization of ACL rupture-induced PTOA utilizing both ^{1}H NMR and DI-MS. Univariate and multivariate analyses indicated that serum concentrations of several acylcarnitine metabolites and tryptophan metabolites differentiate Control and ACLR rats, and these factors may be regulators of the acute and intermediate phases of PTOA. Altered serum levels of carnitine species have been associated with several conditions involving immune dysregulation, including RA.[38] Reduced serum concentration of tryptophan metabolites may further support immune dysregulation in animals with ACL rupture, as decreased levels of tryptophan metabolites are frequently observed in inflammatory arthropathies[37,38] and are associated with increased pro-inflammatory cytokine production[51] and decreased levels of immunomodulating T_{regs}.[43] Glycine, carnosine, and D-mannose were strong metabolites differentiating ACLR from Control rats, and each has been associated with immune and inflammatory conditions.[48–50] The findings from this preliminary investigation indicate a role of immune and inflammatory processes in the response to injury and progressive joint degeneration.

AUTHORS' CONTRIBUTIONS

All authors have made substantial contributions to the conception and design of the study, acquisition of data, or analysis and interpretation of data, as well as manuscript preparation and final approval of the submitted article. KCB takes responsibility for the integrity of the work as a whole.

ACKNOWLEDGMENTS

REFERENCES
1. Little CB, Hunter DJ. 2013. Post-traumatic osteoarthritis: from mouse models to clinical trials. Nat Rev Rheumatol 9:485–497.
2. Lohmander L, Östenberg A, Englund M, et al. 2004. High prevalence of knee osteoarthritis, pain, and functional limitations in female soccer players twelve years after anterior cruciate ligament injury. Arthritis Rheum 50:3145–3152.
3. Svoboda SJ. 2014. ACL injury and posttraumatic osteoarthritis. Clin Sports Med 33:633–640.
4. Von Porat A, Roos E, Roos H. 2004. High prevalence of osteoarthritis 14 years after an anterior cruciate ligament

tear in male soccer players: a study of radiographic and patient relevant outcomes. Ann Rheum Dis 63:269–273.

5. Heard BJ, Solbak NM, Achari Y, et al. 2013. Changes of early post-traumatic osteoarthritis in an ovine model of simulated ACL reconstruction are associated with transient acute post-injury synovial inflammation and tissue catabolism. Osteoarthritis Cartilage 21:1942–1949.

6. O'Brien EJ, Beveridge JE, Huebner KD, et al. 2013. Osteoarthritis develops in the operated joint of an ovine model following ACL reconstruction with immediate anatomic reattachment of the native ACL. J Orthop Res 31:35–43.

7. Tourville TW, Johnson RJ, Slauterbeck JR, et al. 2013. The relationship between synovial fluid ARGS, cytokines, MMPs & TIMPs following acute ACL injury. Osteoarthritis Cartilage 21:S75.

8. Tang Z, Yang L, Zhang J, et al. 2009. Coordinated expression of MMPs and TIMPs in rat knee intra-articular tissues after ACL injury. Connect Tissue Res 50:315–322.

9. Hayward A, Deehan D, Aspden R, et al. 2011. Analysis of sequential cytokine release after ACL reconstruction. Knee Surg Sports Traumatol Arthrosc 19:1709–1715.

10. Wu Y, Yang R, Chen P, et al. 2009. The profile of MMP and TIMP in injured rat ACL. Mol Cell Biomech 7:115–1124.

11. Friel NA, Chu CR. 2013. The role of ACL injury in the development of posttraumatic knee osteoarthritis. Clin Sports Med 32:1–12.

12. Lotz MK. 2010. New developments in osteoarthritis: posttraumatic osteoarthritis: pathogenesis and pharmacological treatment options. Arthritis Res Ther 12:211.

13. Scanzello CR, Goldring SR. 2012. The role of synovitis in osteoarthritis pathogenesis. Bone 51:249–257.

14. Maerz T, Kurdziel M, Newton M, et al. 2016. Subchondral and epiphyseal bone remodeling following surgical transection and noninvasive rupture of the anterior cruciate ligament as models of post-traumatic osteoarthritis. Osteoarthritis Cartilage 24:698–708.

15. Ramme A, Lendhey M, Raya J, et al. 2016. A novel rat model for subchondral microdamage in acute knee injury: a potential mechanism in post-traumatic osteoarthritis. Osteoarthritis Cartilage 24:1776–1785.

16. Anderson DD, Chubinskaya S, Guilak F, et al. 2011. Posttraumatic osteoarthritis: improved understanding and opportunities for early intervention. J Orthop Res 29:802–809.

17. Maerz T, Newton M, Kurdziel M, et al. 2016. Articular cartilage degeneration following anterior cruciate ligament injury: a comparison of surgical transection and noninvasive rupture as preclinical models of post-traumatic osteoarthritis. Osteoarthritis Cartilage 24:1918–1927.

18. Buck R, Wyman B, Le Graverand M-PH, et al. 2010. Osteoarthritis may not be a one-way-road of cartilage loss-comparison of spatial patterns of cartilage change between osteoarthritic and healthy knees. Osteoarthritis Cartilage 18:329–335.

19. Eckstein F, Wirth W, Lohmander L, et al. 2015. Five-Year Followup of Knee Joint Cartilage Thickness Changes After Acute Rupture of the Anterior Cruciate Ligament. Arthritis Rheum 67:152–161.

20. Lotz M, Martel-Pelletier J, Christiansen C, et al. 2013. Value of biomarkers in osteoarthritis: current status and perspectives. Ann Rheum Dis 72:1756–1763.

21. Beckonert O, Keun HC, Ebbels TM, et al. 2007. Metabolic profiling, metabolomic and metabonomic procedures for NMR spectroscopy of urine, plasma, serum and tissue extracts. Nat Protoc 2:2692–2703.

22. Mickiewicz B, Heard BJ, Chau JK, et al. 2015. Metabolic profiling of synovial fluid in a unilateral ovine model of anterior cruciate ligament reconstruction of the knee suggests biomarkers for early osteoarthritis. J Orthop Res 33:71–77.

23. Mickiewicz B, Kelly JJ, Ludwig TE, et al. 2015. Metabolic analysis of knee synovial fluid as a potential diagnostic approach for osteoarthritis. J Orthop Res 33:1631–1638.

24. Zhang W, Sun G, Likhodii S, et al. 2016. Metabolomic analysis of human plasma reveals that arginine is depleted in knee osteoarthritis patients. Osteoarthritis Cartilage 24:827–834.

25. Adams SB, Jr, Setton LA, Nettles DL. 2013. The role of metabolomics in osteoarthritis research. J Am Acad Orthop Surg 21:63.

26. Maerz T, Kurdziel MD, Davidson AA, et al. 2015. Biomechanical characterization of a model of noninvasive, traumatic anterior cruciate ligament injury in the rat. Ann Biomed Eng 43:2467–2476.

27. Maerz T, Fleischer M, Newton MD, et al. 2017. Acute mobilization and migration of bone marrow-derived stem cells following anterior cruciate ligament rupture. Osteoarthritis Cartilage 25:1335–1344.

28. Mercier P, Lewis M, Chang D, et al. 2011. Towards automatic metabolomic profiling of high-resolution one-dimensional proton NMR spectra. J Biomol NMR 49:307–323.

29. Ravanbakhsh S, Liu P, Bjordahl TC, et al. 2015. Accurate, fully-automated NMR spectral profiling for metabolomics. PLoS ONE 10:e0124219.

30. Pan X, Nasaruddin MB, Elliott CT, et al. 2016. Alzheimer's disease-like pathology has transient effects on the brain and blood metabolome. Neurobiol Aging 38:151–163.

31. Xia J, Mandal R, Sinelnikov IV, et al. 2012. MetaboAnalyst 2.0-a comprehensive server for metabolomic data analysis. Nucleic Acids Res 40:W127–W133.

32. Xia J, Sinelnikov IV, Han B, et al. 2015. MetaboAnalyst 3.0-making metabolomics more meaningful. Nucleic Acids Res 43:W251–W257.

33. Tibshirani R. 1996. Regression shrinkage and selection via the lasso. J R Stat Soc Series B Stat Methodol 267–288.

34. Graham SF, Kumar P, Bahado-Singh RO, et al. 2016. Novel metabolite biomarkers of Huntington's disease (HD) as detected by high resolution mass spectrometry. J Proteome Res 15:1592–1601.

35. Grahama SF, Praveen KK, Bjorndahl T, et al. 2016. Metabolic signatures of Huntington's disease (HD): 1H NMR analysis of the polar metabolome in post mortem human brain. Biochim Biophys Acta 1862:1675–1684.

36. Showery JE, Kusnezov NA, Dunn JC, et al. 2016. The rising incidence of degenerative and posttraumatic osteoarthritis of the knee in the United States military. J Arthroplasty 31:2108–2114.

37. Wu T, Xie C, Han J, et al. 2012. Metabolic disturbances associated with systemic lupus erythematosus. PLoS One 7: e37210.

38. van Wietmarschen HA, Dai W, van der Kooij AJ, et al. 2012. Characterization of rheumatoid arthritis subtypes using symptom profiles, clinical chemistry and metabolomics measurements. PLoS ONE 7:e44331.

39. Surowiec I, Arlestig L, Rantapaa-Dahlqvist S, et al. 2016. Metabolite and lipid profiling of biobank plasma samples collected prior to onset of rheumatoid arthritis. PLoS ONE 11:e0164196.

40. Zhang W, Likhodii S, Zhang Y, et al. 2014. Classification of osteoarthritis phenotypes by metabolomics analysis. BMJ Open 4:e006286.

41. Adams SB, Jr., Setton LA, Kensicki E, et al. 2012. Global metabolic profiling of human osteoarthritic synovium. Osteoarthritis Cartilage 20:64–67.

42. Kang KY, Lee SH, Jung SM, et al. 2015. Downregulation of tryptophan-related metabolomic profile in rheumatoid arthritis synovial fluid. J Rheumatol 42:2003–2011.

43. Mezrich JD, Fechner JH, Zhang X, et al. 2010. An interaction between kynurenine and the aryl hydrocarbon receptor can generate regulatory T cells. J Immunol 185:3190–3198.

44. Nguyen NT, Nakahama T, Le DH, et al. 2014. Aryl hydrocarbon receptor and kynurenine: recent advances in autoimmune disease research. Front Immunol 5:551.

45. Chen SY, Wu CL, Lai MD, et al. 2011. Amelioration of rat collagen-induced arthritis through CD4+ T cells apoptosis and synovial interleukin-17 reduction by indoleamine 2,3-dioxygenase gene therapy. Hum Gene Ther 22:145–154.

46. Karasik D, Cheung CL, Zhou Y, et al. 2012. Genome-wide association of an integrated osteoporosis-related phenotype: is there evidence for pleiotropic genes? J Bone Miner Res 27:319–330.

47. Chabbi-Achengli Y, Coman T, Collet C, et al. 2016. Serotonin is involved in autoimmune arthritis through th17 immunity and bone resorption. Am J Pathol 186:927–937.

48. Huffman KM, Jessee R, Andonian B, et al. 2017. Molecular alterations in skeletal muscle in rheumatoid arthritis are related to disease activity, physical inactivity, and disability. Arthritis Res Ther 19:12.

49. Ponist S, Drafi F, Kuncirova V, et al. 2016. Effect of carnosine in experimental arthritis and on primary culture chondrocytes. Oxid Med Cell Longev 2016:8470589.

50. Urita A, Matsuhashi T, Onodera T, et al. 2011. Alterations of high-mannose type N-glycosylation in human and mouse osteoarthritis cartilage. Arthritis Rheum 63:3428–3438.

51. Bertazzo A, Punzi L, Bertazzolo N, et al. 1999. Tryptophan catabolism in synovial fluid of various arthropathies and its relationship with inflammatory cytokines. Adv Exp Med Biol 467:565–570.

SUPPORTING INFORMATION

Additional supporting information may be found in the online version of this article at the publisher's web-site